

CrossMark
click for updatesCite this: *Catal. Sci. Technol.*, 2016,
6, 8325

Al-free Fe-beta as a robust catalyst for selective reduction of nitric oxide by ammonia

Song Song,^a Guangjun Wu,^a Weili Dai,^a Naijia Guan^{ab} and Landong Li^{*ab}

Al-free Fe-beta was prepared from commercial H-beta via a post-synthesis solid-state metallation route and applied as a promising catalyst for selective catalytic reduction of nitric oxide by ammonia. NH₃-TPD and FTIR spectroscopy of pyridine adsorption analysis results clearly verify the absence of Brønsted acid sites and the formation of strong Lewis acid sites in the as-prepared Fe-beta zeolite. Isolated ferric ions within a zeolite framework are determined to be the dominating iron species in Fe-beta according to the characterization results from TEM, H₂-TPR and UV-vis spectroscopy, and these Fe species are exposed and available for reaction as indicated by FTIR spectroscopy of NO adsorption. Fe-beta exhibited good catalytic activity in NH₃-SCR reaction at >573 K, comparable with reference Fe-H-beta prepared via a solid-state ion exchange route, in the presence of SO₂ and excess H₂O. More importantly, Fe-beta exhibited distinctly better durability in NH₃-SCR than reference Fe-H-beta, and a nitrogen oxide conversion of >90% at a reaction temperature of 673 K could be maintained for over 400 h. The remarkable durability of Fe-beta is due to the absence of framework aluminum species and the stabilization of active iron species by the zeolite framework. The reaction mechanism of NH₃-SCR over an Fe-beta model catalyst with well-defined active iron sites was finally investigated by means of *in situ* DRIFT spectroscopy.

Received 8th October 2016,
Accepted 20th October 2016

DOI: 10.1039/c6cy02124g

www.rsc.org/catalysis

1. Introduction

Fe-zeolites have attracted great attention because of their remarkable activities in several very important reactions, *e.g.* the selective catalytic reduction of NO by hydrocarbons (HC-SCR),^{1–5} the selective catalytic reduction of NO by ammonia (NH₃-SCR),^{6–19} the selective catalytic reduction of NO/NO₂ mixtures by ammonia (the so-called fast NH₃-SCR),^{20–25} the catalytic decomposition and/or reduction of N₂O,^{26–33} the N₂O-mediated benzene hydroxylation^{34–37} and the N₂O-mediated oxidative dehydrogenation of propane.^{38–43} Typically, Fe-zeolites are known as commercial NH₃-SCR catalysts for deNO_x from mobile sources, *e.g.* heavy-duty diesel engines,⁴³ and they are also investigated as alternative green catalysts of conventional V₂O₅-WO₃/TiO₂ for deNO_x from stationary sources.

Extensive research studies have been performed on NH₃-SCR catalyzed Fe-zeolites with the focus on the identification of active iron sites, so as to design more active catalysts for the reaction. Despite current achievements, some disagree-

ments do exist and a general conclusion is not drawn yet. In a very early study, Yang *et al.* proposed that isolated Fe²⁺ and the highly-dispersed FeO_x species in Fe/ZSM-5 might contribute to the deNO_x activity in NH₃-SCR, especially at low reaction temperatures.⁹ Iwasaki *et al.* suggested that oxo-Fe³⁺ at the ion-exchanged sites of ZSM-5 zeolites were the active sites for NH₃-SCR, which could be accurately quantified using temperature-programmed desorption of NO₂.¹² Analogously, Sazama *et al.* proposed that Fe³⁺-oxo species with low nuclearity were the most active in NH₃-SCR and the Fe³⁺/Fe²⁺ redox cycle facilitated on these sites due to the charge compensation.¹⁸ Dahl *et al.* believed that iron monomers in Fe-beta were the active species in NH₃-SCR although the monomers were not equally active.¹³ Kröcher *et al.* suggested that all iron species were active in NH₃-SCR catalyzed by Fe-ZSM-5 and their specific activity depended on the reaction temperature.¹⁶ Monomeric species were responsible for the deNO_x activity up to 573 K, while dimeric and oligomeric species and even Fe₂O₃ particles contributed more to the activity at higher temperatures.

In addition to the active sites, the catalytic deactivation of Fe-zeolites is a key issue for NH₃-SCR, especially when considering its practical application. Generally, high-silica zeolites exhibit good hydrothermal stability, however not sufficient for long-term NH₃-SCR reaction (with ~10% steam). Thereupon, the hydrothermal deactivation of Fe-zeolites is a common phenomenon in the NH₃-SCR process, while the

^aSchool of Materials Science and Engineering & National Institute for Advanced Materials, Nankai University, Tianjin, 300350, PR China.

E-mail: lild@nankai.edu.cn; Fax: +86 22 23500341; Tel: +86 22 23500341

^bKey Laboratory of Advanced Energy Materials Chemistry (Ministry of Education), Collaborative Innovation Center of Chemical Science and Engineering, Tianjin, 300071, PR China

detailed mechanism of deactivation is somewhat complicated. For example, the extensive detachment of Fe species from the ion-exchange positions upon zeolite dealumination was observed by Makkee *et al.*,⁴⁴ which accordingly resulted in the deactivation of Fe-ZSM-5. Toops *et al.* confirmed the activity loss of Fe-zeolite due to catalyst deterioration during NH₃-SCR at elevated temperatures, as reflected by the surface area losses, zeolite dealumination and Fe₂O₃ crystal growth.⁴⁵ Kröcher *et al.* established the deactivation mechanism of Fe-ZSM-5 in NH₃-SCR with three distinct causes, *i.e.* the quick zeolite dealumination, the rapid loss of iron dimers and the migration of iron monomers triggered by zeolite dealumination.¹⁵

On the basis of the above-mentioned issues, it can be proposed that the framework Al species in zeolites were related to both the catalytically active Fe sites for NH₃-SCR and the deactivation of Fe-zeolites during the reaction. The presence of framework Al species can directly influence the distribution of Fe species in the zeolite,^{17,18,31} and also increase the difficulty in the identification of Fe sites. On the other hand, catalyst deactivation caused by the aggregation and/or the detachment of Fe species upon framework dealumination could not be avoided. Generally, Brønsted acid sites from framework Al species in Fe-zeolites are recognized as a necessary NH₃ reservoir for NH₃-SCR. However, it has been also argued that Brønsted acidity is not required for adsorbing or activating the ammonia and, therefore, not a crucial factor for high NH₃-SCR activity.¹⁴ Inspired by intense previous research studies, we herein design Al-free Fe-beta for NH₃-SCR with the purpose of eliminating the impacts from framework Al species on the catalytic activity and deactivation. The Al-free Fe-beta sample is prepared *via* a post-synthesis metallation route developed by Dzwigaj *et al.*^{46,47} with our own modifications by using organometallic precursors to obtain well isolated sites in a zeolite matrix.^{48,49} The catalytic and deactivation behaviors of the as-prepared Fe-beta will be the focus of this study, and the NH₃-SCR reaction mechanism will be discussed.

2. Experimental section

2.1 Catalyst preparation

Fe-beta was prepared *via* the so-called solid-state metallation route, including the dealumination of an aluminosilicate zeolite and the subsequent incorporation of Fe into a zeolite framework. Commercial H-beta zeolite from Sinopec Co. (Si/Al = 13.5) was first treated with concentrated nitric acid (13 M) to obtain Al-free Si-beta. After thoroughly washing and drying at 353 K, 0.5 g of Si-beta zeolite was ground with 0.1 g of ferrocene (FeCp₂) to obtain the well-mixed solid, which was then calcined in flowing 5% O₂/Ar at increasing temperatures from 298 to 873 K to derive Fe-beta.

For reference, Fe-H-beta was prepared *via* a solid-state ion exchange route. In a typical experiment, 0.5 g of calcined H-beta zeolite sample was ground with 0.1 g of FeCl₃ in the glove box and then transferred to a sealed ceramic container

for heating at 573 K for 2 h. After washing and drying, the obtained solid material was calcined in flowing 5% O₂/Ar at 873 K for 6 h.

2.2 Catalyst characterization

The Si, Al and Fe loadings in zeolite samples were analyzed by using a Perkin Elmer Optima 2000 inductively coupled plasma optical emission spectrometer (ICP-OES).

The specific surface areas of the zeolite samples were determined using a Quantachrome iQ-MP gas adsorption analyzer through low temperature N₂ adsorption/desorption isotherms.

The X-ray diffraction (XRD) patterns of zeolite samples were recorded on a Bruker D8 ADVANCE powder diffractometer with Cu-K radiation ($\lambda = 0.1542$ nm) at a scanning rate of 4° min⁻¹ in the region of $2\theta = 5\text{--}40^\circ$.

Transmission electron microscopy (TEM), high-resolution transmission electron microscopy (HR-TEM) and high-angle angular-dark-field transmission electron microscopy (HAADF STEM) images of Fe-zeolites were obtained using a FEI Tecnai G² F20 electron microscope at an acceleration voltage of 200 kV. A few drops of alcohol suspension containing the sample were placed on a carbon-coated copper grid, followed by evaporation at ambient temperature.

Fourier transform infrared (FTIR) spectra of samples were measured using a Bruker Tensor 27 spectrometer with 128 scans at a resolution of 2 cm⁻¹. A self-supporting pellet made of the sample was placed in the reaction chamber and heated to designated temperatures for recording the spectra against KBr as background.

Diffuse reflectance ultraviolet-visible (UV-vis) spectra of Fe-zeolites (diluted in BaSO₄) were recorded in air against BaSO₄ in the region of 200–800 nm on a Varian Cary 300 UV-vis spectrophotometer.

The temperature-programmed reduction (TPR) experiments were carried out using a Quantachrome ChemBET 3000 chemisorption analyzer. An Fe-zeolite sample of *ca.* 0.1 g was pretreated in flowing 5% O₂/Ar at 873 K for 1 h, cooled to 323 K under the same atmosphere and purged with 5% H₂/Ar for 30 min. H₂-TPR was then carried out in flowing 5% H₂/Ar in the temperature range of 323–873 K at a heating rate of 10 K min⁻¹.

The temperature-programmed desorption (TPD) experiments were carried out using a Quantachrome ChemBET 3000 chemisorption analyzer. A sample of *ca.* 0.1 g was pretreated in flowing 5% O₂/Ar at 873 K for 1 h, cooled to 373 K in He and saturated with 5% NH₃/He. After that, the sample was purged with He for 30 min to eliminate the physisorbed ammonia. NH₃-TPD was then carried out in flowing He in the temperature range of 373–873 K at a heating rate of 10 K min⁻¹.

FTIR spectra with NO as a probe were collected using a Bruker Tensor 27 spectrometer with 128 scans at a resolution of 2 cm⁻¹. A self-supporting pellet made of the Fe-zeolite sample was placed in the reaction chamber and pretreated in

flowing He at 773 K for 1 h. After cooling to room temperature in flowing He, the He stream was switched to 0.1% NO/He and a series of time-dependent FTIR spectra were sequentially recorded.

FTIR spectra of pyridine adsorption were also collected using the Bruker Tensor 27 spectrometer with 128 scans at a resolution of 2 cm⁻¹. A self-supporting pellet made of the sample was placed in the flow cell and evacuated at 673 K for 4 h. After cooling to room temperature, the samples were saturated with pyridine vapor and then evacuated at 473 K for 1 h. The spectra were recorded at the evacuation temperature in the 4000–650 cm⁻¹ range. Quantitative analysis was performed using the method of Emeis.⁵⁰

2.3 Catalytic study

The NH₃-SCR reaction was performed in a fixed-bed micro-reactor (Tianjin Golden Eagle Technology Co.) at atmospheric pressure. In a typical process, 0.2 g of catalyst sample (sieve fraction 250–400 μm) was placed in a quartz reactor (6 mm internal diameter) and treated in 5% O₂/Ar at 873 K for 1 h. After cooling to the designated temperature in He, the reactant gas mixture (NO = 1000 ppm; NH₃ = 1000 ppm; O₂ = 10%; SO₂ = 50 ppm; H₂O = 10%, He balance) was fed to the sample. The total flow rate is 200 mL min⁻¹, corresponding to a gas hourly space velocity (GHSV) of 60 000 per h. The outlet from the reactor was analyzed online using a mass spectrometer (Pfeiffer Omnistar). The following main mass fragments (*m/z*) were analyzed: 4 (He), 17 (NH₃), 18 (H₂O), 28 (N₂, N₂O), 30 (NO, NO₂, N₂O), 44 (N₂O), 46 (NO₂). The outlet concentrations of NH₃, NO and NO₂ were also monitored by using a gas analyzer (Fodisch MCA04). The conversion, selectivity and yield are defined as follows (NO_x = NO + NO₂):

$$\text{NO}_x \text{ conversion (\%)} = \frac{[\text{NO}_x]_{\text{inlet}} - [\text{NO}_x]_{\text{outlet}}}{[\text{NO}_x]_{\text{inlet}}} \times 100\%$$

$$\text{NH}_3 \text{ conversion (\%)} = \frac{[\text{NH}_3]_{\text{inlet}} - [\text{NH}_3]_{\text{outlet}}}{[\text{NH}_3]_{\text{inlet}}} \times 100\%$$

$$\text{N}_2 \text{ selectivity (\%)} = \frac{2 \times [\text{N}_2]_{\text{outlet}}}{[\text{NO}_x]_{\text{inlet}} - [\text{NO}_x]_{\text{outlet}}} \times 100\%$$

2.4 In situ DRIFT study

In situ diffuse reflectance infrared Fourier transform (DRIFT) spectra were also measured using the Bruker Tensor 27 spectrometer, with a liquid nitrogen cooled high sensitivity mercury cadmium telluride detector. In a typical experiment, a catalyst sample of ~25 mg loose powder was placed in the chamber and treated in 5% O₂/Ar at 773 K for 1 h. After

cooling to the designated temperature, the reaction gas mixture (1000 ppm NO, 1000 ppm NH₃, 10% O₂, He balance, 25 mL min⁻¹) was fed, and the time-dependent spectra were recorded with a resolution of 4 cm⁻¹.

3. Results and discussion

3.1 Preparation of Fe-beta via post-synthesis metallation

The possible incorporation of Fe species into the framework of Si-beta is first monitored by FTIR spectroscopy, and the results are shown in Fig. 1. In the initial sample of FeCp₂/Si-beta, isolated silanol groups (3730 cm⁻¹), hydroxyls at defect sites (3660 cm⁻¹), hydrogen-bonded silanol groups (3200–3600 cm⁻¹)⁴⁹ and cyclopentadienyl groups (stretching vibration of =C–H and C=C at 3120 and 1630 cm⁻¹, respectively⁵¹) could be clearly identified. Heating in flowing O₂/Ar resulted in a gradual loss of cyclopentadienyl groups *via* the formation CO₂, as disclosed by the IR bands occurring at 2300 and 2360 cm⁻¹. Accompanied by the loss of cyclopentadienyl groups, the IR band corresponding to the hydroxyls at defect sites disappears and the intensity of the hydrogen-bonded silanol groups decreases dramatically, indicating the reaction between FeCp₂ and these groups. According to the temperature-resolved FTIR spectra, the reaction between FeCp₂ and the silanol groups should be completed below 673 K and Fe species are expected to be incorporated into the BEA framework.

Fig. 2 shows the XRD patterns of H-beta, Si-beta, Fe-beta and reference Fe–H-beta. All the samples show typical diffraction peaks characteristic of typical BEA topology. Obviously, the beta zeolite framework could be well preserved after dealumination and introduction of Fe species through metallation or solid-state ion exchange. Bulk iron oxide formation could be excluded from the absence of the corresponding

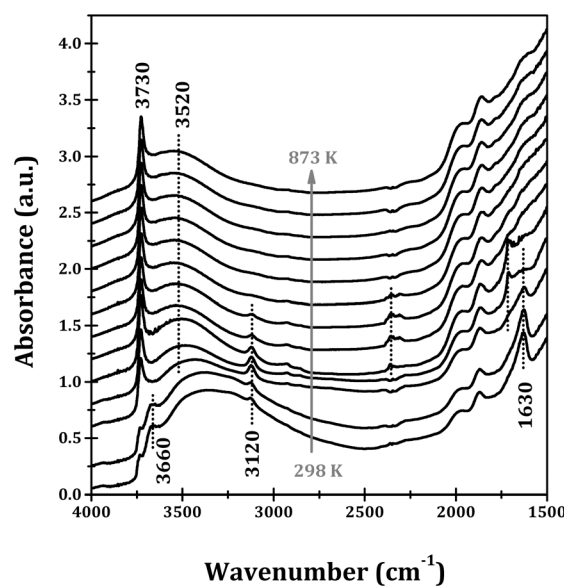


Fig. 1 FTIR spectra of FeCp₂/Si-beta in flowing 5% O₂/Ar at increasing temperatures from 298 to 873 K.

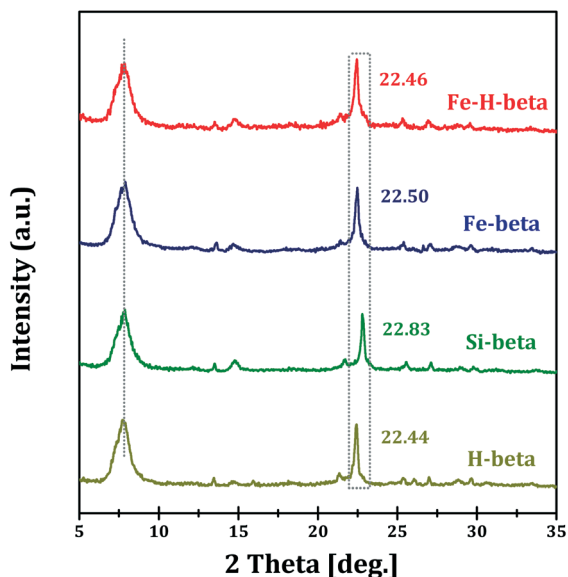


Fig. 2 XRD patterns of H-beta, Si-beta, Fe-beta and Fe-H-beta.

diffraction peaks. It has been proposed by Dzwigaj *et al.* that the dealumination and metal ion incorporation into the BEA zeolite framework should be accompanied by the contraction/expansion of the framework, which accordingly resulted in detectable changes in the position of the (302) diffraction peak ($2\theta = \sim 22.5^\circ$).^{46,47} In our study, the d_{302} spacing, calculated from the corresponding 2θ value, decreased from 3.954 Å (H-beta, $2\theta = 22.44^\circ$) to 3.896 Å (Si-beta, $2\theta = 22.83^\circ$) through dealumination, while it increased to 3.927 Å (Fe-beta, $2\theta = 22.50^\circ$) after Fe incorporation. These experimental observations support the incorporation of Fe species into the BEA zeolite framework *via* post-synthesis metallation.

The acidic properties of Fe-beta and reference Fe-H-beta are evaluated by means of NH_3 -TPD and FTIR spectra of pyri-

dine adsorption. As shown in Fig. 3, two major ammonia desorption peaks can be distinguished for H-beta, *i.e.* one peak centered at ~ 500 K due to weak acid sites and one peak at ~ 650 K due to strong acid sites. Both of these acid sites disappear after the complete removal of framework Al species, *i.e.* Si-beta. Upon Fe species incorporation into the framework (Fe-beta), the acid sites recover to some extent, and a low-temperature peak at ~ 500 K corresponding to weak acid sites as well as a high-temperature peak at ~ 600 K corresponding to moderate acid sites could be observed. However, the amounts of acid sites are distinctly lower than parent H-beta and the acid strength changed. The creation of moderate acid sites in Fe-beta compared with Si-beta further confirms the incorporation of Fe species into the zeolite framework. For Fe-H-beta prepared by solid-state ion exchange, both weak acid sites (ammonia desorption peak centered at ~ 500 K) and strong acid sites (ammonia desorption peak centered at ~ 650 K) could be observed, similar to the case of parent H-beta.

For further information on the amount and type of acid sites in Fe-zeolites, FTIR spectra of pyridine adsorption are recorded. Pyridine molecules could, in principle, react with the protons (Brønsted acid sites) to form pyridinium ions (characterized by IR bands from 1512 to 1567 cm^{-1}) and/or interact with the Lewis acid sites through their isolated electron pairs in nitrogen atoms (characterized by IR bands from 1423 to 1472 cm^{-1}).^{50,52}

Both Brønsted acid and Lewis acid sites are present in H-beta samples, while all the acid sites completely disappear after complete dealumination (Si-beta).⁴⁸ Upon the incorporation of Fe species into the BEA framework, new Lewis acid sites originating from Fe species are created, as indicated by the appearance of an IR band at ~ 1450 cm^{-1} (Fig. 4). Most of the newly-created Lewis acid sites are strong Lewis acid sites

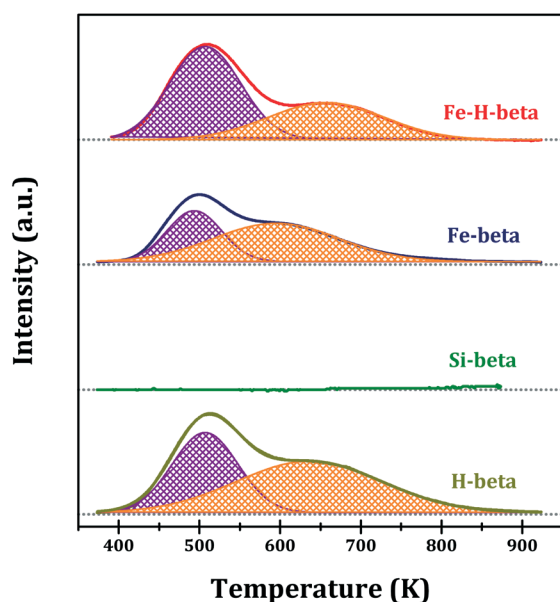


Fig. 3 NH_3 -TPD profiles of Fe-beta and Fe-H-beta.

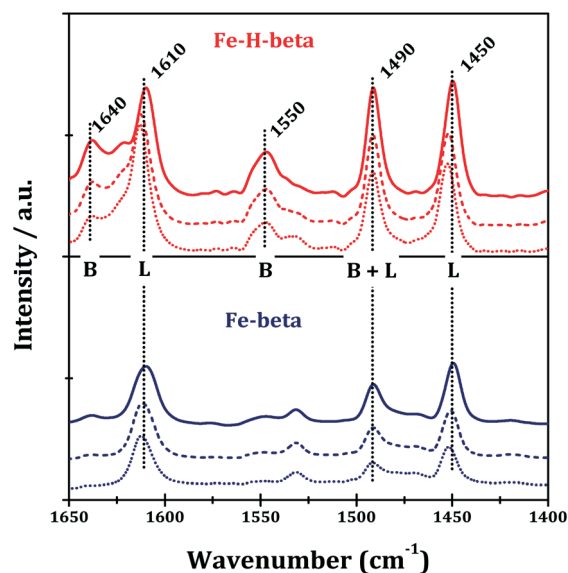


Fig. 4 FTIR spectra of Fe-beta and Fe-H-beta after pyridine adsorption followed by evacuation at 473 (solid line), 573 (dashed line) and 623 K (dotted line).

that can survive from evacuation at 623 K. In fact, the as-prepared Fe-beta exhibited good catalytic activity in the Meerwein-Ponndorf-Verley reduction of ethyl levulinate by isopropanol to γ -valerolactone (ethyl levulinate conversion rate of $3.8 \text{ mmol g}_{\text{cat}}^{-1} \text{ h}^{-1}$ and γ -valerolactone selectivity of 90% at 423 K), a typical reaction catalyzed by Lewis acids,⁵³ confirming the formation of catalytically active Lewis acid sites in Fe-beta. While for Fe-H-beta, both Brønsted acid (IR bands at $\sim 1550 \text{ cm}^{-1}$) and Lewis acid sites (IR bands at $\sim 1450 \text{ cm}^{-1}$) could be observed. The quantitative analysis results on the acid sites in Fe-zeolites are summarized in Table 1.

On the basis of these results, it can be stated that Al-free Fe-beta, free of Brønsted acid sites, has been successfully prepared *via* the post-synthesis metallation route. It should be mentioned that although Fe species are expected to replace framework Al species through the post-synthesis metallation route, the chemical environments of Fe might be different from the Al precursors. One framework Al atom is connected with four $-\text{O}-\text{Si}-$ linkages, forming closed structure $\text{Al}(\text{SiO})_4$. While the Fe atom might connect with one, two or three $-\text{O}-\text{Si}-$ linkages, forming open structure $\text{Fe}(\text{SiO})$, $\text{Fe}(\text{SiO})_2$ or $\text{Fe}(\text{SiO})_3$, respectively, similar to the case of Sn-zeolite.⁵⁴ Under such circumstances, Lewis acid sites instead of Brønsted acid sites are created by Fe incorporation into the zeolite framework, as confirmed by NH_3 -TPD (Fig. 3) and FTIR spectra of pyridine adsorption (Fig. 4).

3.2 Investigation of iron sites in zeolites

The distribution of Fe species in Fe-beta is directly observed by electron microscopy. In the HR-TEM image of Fe-beta (Fig. 5a), fine crystal lattice fringes of BEA zeolite are clearly observed and no Fe-containing particles could be identified, although the presence of 4.8% Fe is revealed by the selected-area energy dispersive spectroscopy analysis (Fig. 5b). That is, the Fe species should exist in the form of sub-nanometre compounds, *e.g.* monomers or dimers. In the HAADF-STEM image of Fe-beta (Fig. 5c) and the corresponding element mappings (Fig. 5d), the homogeneous distribution of isolated Fe species without surface enrichment of Fe species is further confirmed. It should be noted that the distribution of Fe species in Fe-beta could be well preserved even after long-term NH_3 -SCR for 400 h and no sign of Fe particle aggregation appears (Fig. 5e), which might be related to the remarkable durability of the Fe-beta catalyst (*vide infra*). For comparison,

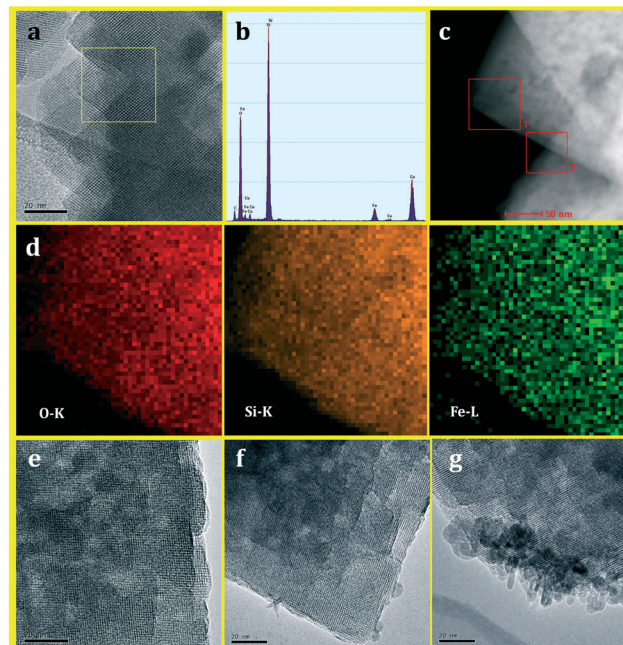


Fig. 5 HR-TEM image of Fe-beta (a) and selected area EDX analysis (b); HAADF-STEM image of Fe-beta (c) with the corresponding element mapping analysis (d); HR-TEM image of Fe-beta (e) after long-term NH_3 -SCR for 400 h; HR-TEM image of Fe-H-beta before (f) and after (g) long-term NH_3 -SCR for 400 h.

the HR-TEM images of Fe-H-beta before and after NH_3 -SCR are shown. Typically, irregular nanoparticles of 2–5 nm could be observed on the zeolite support, indicating the existence of oligonuclear Fe_xO_y clusters and Fe_2O_3 nanoparticles in the as-prepared Fe-H-beta (Fig. 5f). Some isolated Fe species might also exist, similar to the case of Fe-beta; however, they are invisible in the HR-TEM image. Through NH_3 -SCR reaction, distinct aggregation of Fe species occurs and large particles up to 20 nm are observed at the edges of the beta crystals (Fig. 5g). This might be due to the growth of the iron oxides induced by the existence of extra-framework aluminum species from dealumination as suggested by Prins *et al.*,⁵⁵ which is a common phenomenon for Al-containing Fe-zeolites. Obviously, the Fe species in Fe-H-beta are not stable and a loss of catalytic activity in NH_3 -SCR reaction could be predicted. ICP analysis further reveals that the Fe content in Fe-beta remains nearly unchanged after long-term NH_3 -SCR reaction, while close to half Fe species in Fe-H-beta flow away during the reaction (Table 1).

Table 1 Physicochemical properties of Fe-zeolite samples under study

Sample	Si/Al/Fe ^b (%)	Brønsted acid ^c ($\mu\text{mol g}^{-1}$)	Lewis acid ^c ($\mu\text{mol g}^{-1}$)	Fe_xO_y size ^d (nm)	S_{BET} ($\text{m}^2 \text{g}^{-1}$)
Fe-beta	45.8/<0.1/5.1	0	230	<0.5	577
Fe-beta ^a	45.7/<0.1/4.9	—	—	<0.5	536
Fe-H-beta	45.5/3.2/5.7	180	420	3.0	564
Fe-H-beta ^a	45.1/3.1/2.9	—	—	15.8	321

^a After NH_3 -SCR reaction at 673 K for 400 h. ^b Determined by ICP analysis. ^c Determined by FTIR spectra of pyridine adsorption followed by evacuation at 623 K. ^d Typical size observed by TEM.

The nature of Fe species in Fe-beta and Fe-H-beta is investigated by H₂-TPR. For Fe-beta, a dominating H₂ consumption peak at 523–773 K (H/Fe = ~1.0) as well as a minor small H₂ consumption peak at 673–973 K (H/Fe = ~0.1) could be identified (Fig. 6). The former peak should come from the reduction of isolated Fe³⁺ to Fe²⁺ while the latter one from the reduction of Fe_xO_y clusters.^{10,15} The further reduction of isolated Fe²⁺ interacting with the zeolite framework occurs at over 973 K accompanied by the collapse of the zeolite framework and it will not be discussed here. For Fe-H-beta, a two stage reduction of Fe species is also observed, *i.e.* the reduction of isolated Fe³⁺ to Fe²⁺ (H/Fe = ~1.0) and the reduction of Fe_xO_y clusters (H/Fe = ~0.9). It should be mentioned that the peak from the reduction of isolated Fe³⁺ to Fe²⁺ is distinctly broader for Fe-beta than that for Fe-H-beta. This might be due to the formation of different interactions between Fe³⁺ species and the zeolite framework in the case of Fe-beta. The H₂-TPR and quantitative analysis results reveal that the isolated Fe³⁺ are the dominating species in Fe-beta, while a significant amount of Fe_xO_y clusters is present in Fe-H-beta, consistent with TEM observations.

Fig. 7 displays the UV-vis spectra of Fe-beta and Fe-H-beta before and after NH₃-SCR reaction. For Fe-beta, strong absorbance is observed between 33 300 and 50 000 cm⁻¹ (200–300 nm) and it should be caused by isolated ferric ions in tetrahedral and/or octahedral coordination.^{37,56} The UV-vis spectrum of Fe-beta after long-term NH₃-SCR is quite similar to that before the reaction, and the Fe species remained in the isolated states during the reaction. While for Fe-H-beta, absorbance in the wide range of 15 000 to 50 000 cm⁻¹ is observed, revealing the existence of isolated ferric ions (33 300–50 000 cm⁻¹), oligonuclear Fe_xO_y clusters (25 000–33 300 cm⁻¹) and large Fe₂O₃ nanoparticles (15 000–25 000 cm⁻¹). After long-term NH₃-SCR reaction, the absorbance intensity in the wide range

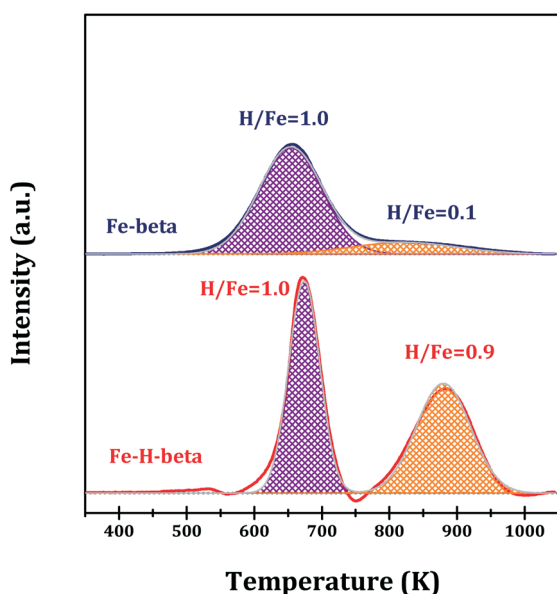


Fig. 6 H₂-TPR profiles of Fe-beta and Fe-H-beta.

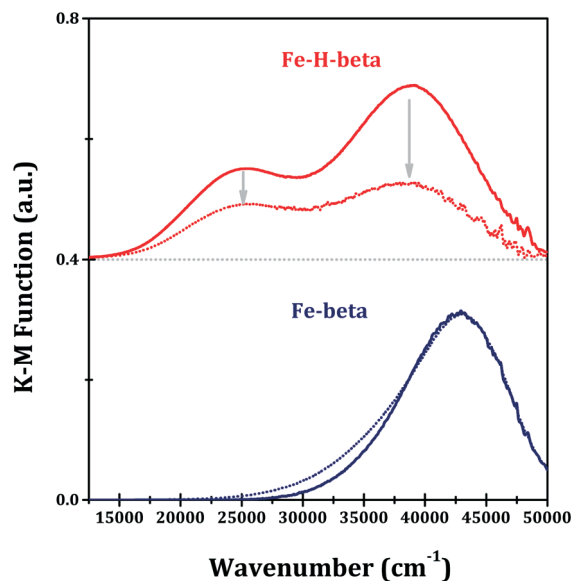


Fig. 7 UV-vis spectra of Fe-beta and Fe-H-beta before (solid line) and after (dotted line) NH₃-SCR reaction.

decreases distinctly due to the loss of Fe species during the reaction (Table 1). Meanwhile, a more pronounced decrease in the absorbance from isolated ferric ions (33 300–50 000 cm⁻¹) is observed, hinting the transformation of isolated ions to oligonuclear Fe_xO_y clusters and/or large Fe₂O₃ particles during NH₃-SCR reaction.

FTIR spectroscopy of NO adsorption is further employed to provide information on the exposed sites in Fe-zeolites. NO adsorption on Fe-H-beta brings about a dominating IR band at ~1870 cm⁻¹ and a shoulder IR band at ~1850 cm⁻¹ (Fig. 8), assignable to mono-nitrosyls on extra-framework Fe²⁺-O-Al species^{57,58} and isolated ferrous ions,⁵⁹ respectively. Since Fe-H-beta was prepared from the solid-state ion exchange route, it is rational to obtain extra-framework Fe²⁺-O-Al as the dominating available species in Fe-H-beta. In contrast, NO adsorption on Fe-beta gives a dominating band at ~1855 cm⁻¹ from mono-nitrosyls on isolated ferrous ions, accompanied by weak shoulder bands at 1810–1830 cm⁻¹

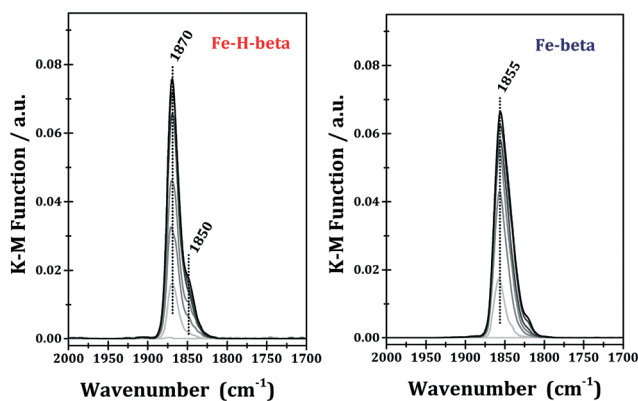


Fig. 8 Time-resolved FTIR spectra of NO adsorption on Fe-beta and Fe-H-beta from 0 to 10 min.

corresponding to poly-nitrosyls on isolated ferrous ions, *i.e.* $\text{Fe}^{2+}(\text{NO})_n$, $n \geq 2$.⁵⁷ Obviously, isolated ferric ions are exposed iron species in Fe-beta, in good agreement with UV-vis analysis results. According to the FTIR spectra of NO adsorption, quite distinct iron species (exposed) are formed in Fe-H-beta and Fe-beta with different chemical constitutions (Al-containing and Al-free) and prepared *via* different routes (solid-state ion exchange and solid-state metallation).

3.3 NH_3 -SCR catalyzed by Fe-beta and Fe-H-beta

The as-prepared Fe-beta, together with reference Fe-H-beta and H-beta, is investigated as a catalyst for NH_3 -SCR reaction, and the results are shown in Fig. 9. Considering the practical application of Fe-beta, excess water vapour (10%) and SO_2 (50 ppm) are included in the reactant mixture. H-beta exhibits considerable activity in NH_3 -SCR with maximal NO_x conversion of $\sim 23\%$ at 723 K, and the activity might come from the Fe impurity in the sample.^{60,61} Both Fe-beta and Fe-H-beta exhibit remarkable catalytic activity in standard NH_3 -SCR, and maximal NO_x conversions of $>90\%$ are achieved at 673 K.

Obviously, the extra Fe species introduced to H-beta play a dominating role in NH_3 -SCR reaction. With a similar Fe content, Fe-H-beta exhibits similar deNO_x activity to Fe-beta in the temperature range of 623–723 K, while it exhibits distinctly higher deNO_x activity at low temperatures. It should be noted that only traces of N_2O are detected as a by-product from NO_x reduction (N_2 selectivity $>90\%$), and it is not discussed here. Nevertheless, Fe-beta is an adequate catalyst for practical NH_3 -SCR at 623–723 K. Moreover, Fe-beta exhibits better stability than Fe-H-beta, and only a very slight activity loss in NH_3 -SCR can be observed after hydrothermal aging (973 K for 12 h, labelled as aged Fe-beta in Fig. 9).

According to the characterization results, various Fe species as well as residual Brønsted acid sites exist in Fe-H-beta prepared *via* the solid-state ion exchange route and it is very difficult to disclose their respective functions in NH_3 -SCR reaction. In contrast, isolated ferric ions stabilized in the zeolite framework are detected as the dominating species in Fe-beta and they are the only possible active sites for NH_3 -SCR. The ratios between reacted NH_3 and reacted NO_x over Fe-

beta, Fe-H-beta and H-beta are calculated and shown in Fig. 10. Since the equimolar reaction between NO_x and NH_3 is known for both NH_3 -SCR ($4\text{NH}_3 + 4\text{NO} + \text{O}_2 \rightarrow 4\text{N}_2 + 6\text{H}_2\text{O}$) and fast NH_3 -SCR ($2\text{NH}_3 + \text{NO} + \text{NO}_2 \rightarrow 2\text{N}_2 + 3\text{H}_2\text{O}$), the excess consumption of NH_3 , *i.e.* $\text{NH}_3/\text{NO}_x > 1$, comes from the oxidation by O_2 in the reaction system ($4\text{NH}_3 + 5\text{O}_2 \rightarrow 4\text{N}_2 + 6\text{H}_2\text{O}$). The NH_3/NO_x ratio over H-beta appears to be distinctly higher than those of Fe-beta and Fe-H-beta in the temperature range of 623–723 K, indicating that Brønsted acid sites may facilitate the direct oxidation of NH_3 by O_2 . Moreover, it has been reported by Shen *et al.* that Fe oligomers in Fe-zeolites are active for NH_3 oxidation,⁶² which might be another reason for the higher NH_3/NO_x over Fe-H-beta than that over Fe-beta.

The long-term durability of Fe-beta and that of Fe-H-beta in NH_3 -SCR are further investigated. As shown in Fig. 11, Fe-beta exhibits remarkable stability and no activity loss could be observed for as long as 400 h. In contrast, a gradual loss of activity is observed for Fe-H-beta and the NO_x conversion decreases from 92% to below 70% within 400 h. The general issues leading to catalytic deactivation, *i.e.* zeolite framework dealumination and the consequent Fe aggregation, could be avoided by using Al-free Fe-beta as a catalyst as compared to Fe-H-beta. Moreover, the active ferric ions in Fe-beta are efficiently stabilized by the zeolite framework for NH_3 -SCR. As a result, the stable high NO_x conversion of $>90\%$ at 673 K in the presence of both water vapour and SO_2 is achieved with Fe-beta, which appears readily practical for NH_3 -SCR application.

3.4 Reaction mechanism of NH_3 -SCR over Fe-beta

With adequate information on the active Fe species, it becomes easier to investigate the NH_3 -SCR reaction mechanism

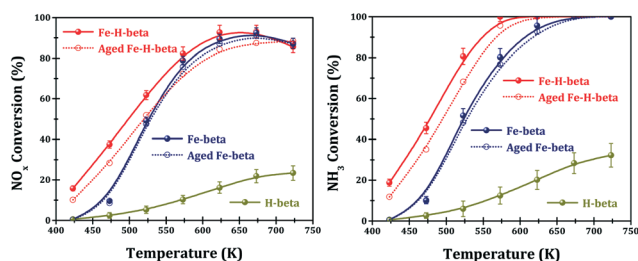


Fig. 9 NH_3 -SCR catalyzed by Fe-beta and Fe-H-beta. Reaction conditions: $\text{NO} = 1000$ ppm; $\text{NH}_3 = 1000$ ppm; $\text{O}_2 = 10\%$; $\text{SO}_2 = 50$ ppm; $\text{H}_2\text{O} = 10\%$; 0.2 g catalyst; total flow rates of 200 mL min^{-1} ; GHSV of 60 000 per h.

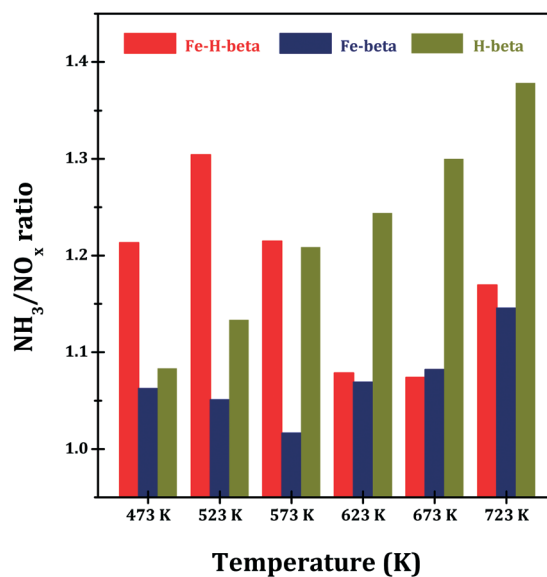


Fig. 10 The ratios between reacted NH_3 and reacted NO_x during NH_3 -SCR catalyzed by Fe-beta and Fe-H-beta.

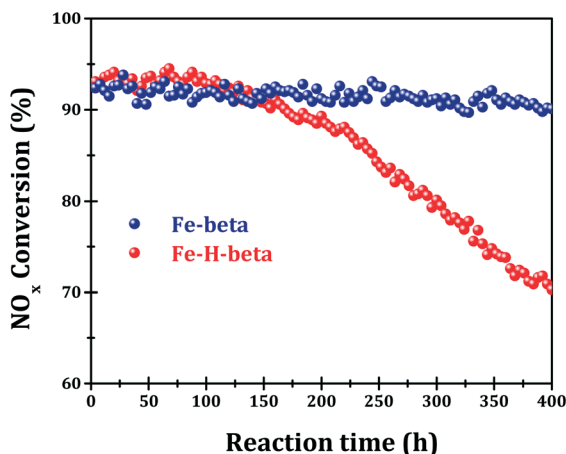


Fig. 11 Durability test of NH_3 -SCR over Fe-beta and Fe-H-beta at 673 K. Reaction conditions: $\text{NO} = 1000$ ppm; $\text{NH}_3 = 1000$ ppm; $\text{O}_2 = 10\%$; $\text{SO}_2 = 50$ ppm; $\text{H}_2\text{O} = 10\%$, 0.2 g catalyst, total flow rates of 200 mL min^{-1} , GHSV of $60\,000$ per h.

over a model Fe-beta catalyst than that over Fe-H-beta with complicated Fe species composition (in fact, it is quite difficult to obtain reliable information on the NH_3 -SCR mechanism over Fe-H-beta due to the overlap of various spectroscopy signals from different Fe species). For Al-free Fe-beta zeolite, all iron species are stabilized by the zeolite framework, and therefore, the location changes of Fe species during NH_3 -SCR reaction, as observed by Lercher *et al.*,^{63,64} would not happen in our case.

In situ DRIFT spectra obtained in the NO - NH_3 - O_2 reaction system over Fe-beta are shown in Fig. 12 (water vapour and SO_2 are not included in the reactant mixture to avoid their interference on spectroscopy signals). In flowing NO at 673 K, a strong IR band at $\sim 1850 \text{ cm}^{-1}$ due to mono-nitrosyls on isolated ferrous ions is observed, similar to that observed at

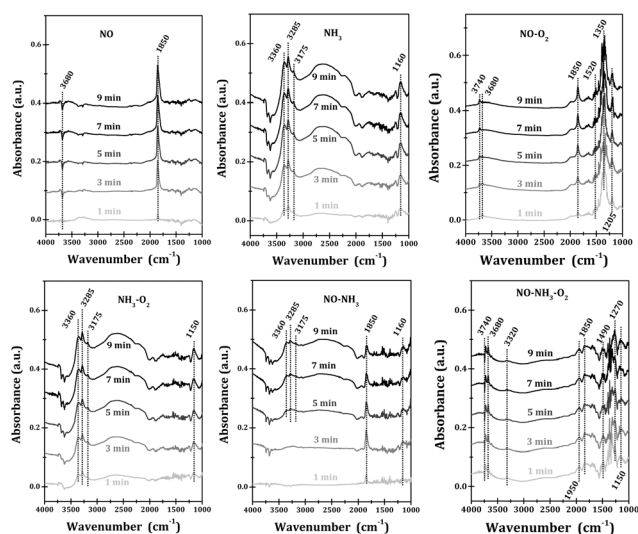


Fig. 12 *In situ* DRIFT spectra of the NO - NH_3 - O_2 reaction system over Fe-beta at 673 K. Reaction conditions: $\text{NO} = 1000$ ppm; $\text{NH}_3 = 1000$ ppm; $\text{O}_2 = 10\%$; ~ 25 mg catalyst; total flow rates of 25 mL min^{-1} ; GHSV = $\sim 60\,000$ per h.

room temperature (Fig. 8). Meanwhile, a negative band at 3680 cm^{-1} due to hydroxyls bounded to iron sites is observed upon NO adsorption. Obviously, mono-nitrosyls can interact with iron sites and result in the reduction of hydroxyls on them. In flowing NH_3 , a series of bands in the range of 3500 – 3100 cm^{-1} are observed, corresponding to the asymmetric stretching (3360 cm^{-1}) and symmetric stretching (3285 and 3175 cm^{-1}) vibrations of NH_3 on Lewis acid sites, respectively.^{65,66} The band at 1160 cm^{-1} due to the asymmetric bending vibrations of NH_3 on Lewis acid sites is also observed. Besides, a series of negative bands in the range of 4000 – 3500 cm^{-1} are observed, which originated from the eradication of hydroxyls by H-bonding with ammonia.⁶⁷ With the co-feeding of NH_3 and O_2 to Fe-beta, the surface species formed are almost the same as those observed from feeding NH_3 alone. Mass spectrum analysis results clearly indicate the formation of N_2 as the dominating product from NH_3 oxidation by O_2 at 673 K. In flowing NO - O_2 , a series of IR bands corresponding to N_xO_y species can be observed, e.g. the band at 1520 cm^{-1} due to nitrates, the band at $\sim 1350 \text{ cm}^{-1}$ due to nitro compounds and the band at 1205 cm^{-1} due to nitrites.⁶⁸ It is therefore proposed that mono-nitrosyls on isolated ferrous ions (IR band at 1850 cm^{-1}) could be easily oxidized by oxygen to N_xO_y species. Since ferrous ions can be synchronously oxidized to ferric ions, hydroxyls will be formed on the ferric ions, as revealed by the appearance of an IR band at 3680 cm^{-1} . With the co-feeding of NH_3 and NO to Fe-beta, mono-nitrosyls on ferrous ions (IR band at 1850 cm^{-1}) were immediately observed and NH_3 species on Lewis acid sites (IR bands at 3360 , 3285 , 3175 and 1160 cm^{-1}) appeared afterward, at the expense of mono-nitrosyls. These observations clearly suggest that NH_3 and NO compete for the same adsorption sites, *i.e.* the iron sites, during the reaction. The reaction between NH_3 and NO (in the absence of O_2) is slow and only a small quantity of N_2 and N_2O product could be detected, *i.e.* NO conversion $< 20\%$. Under simulated NH_3 -SCR reaction conditions, *i.e.* NH_3 - NO - O_2 , IR bands due to NH species (3320 cm^{-1}),⁶⁹ associated nitrosyls (1950 cm^{-1}),⁶⁸ mono-nitrosyls (1850 cm^{-1}), nitroxyl HNO species (1490 cm^{-1}),⁷⁰ free nitrites (1270 cm^{-1})⁷¹ and chelating nitrites (1150 cm^{-1})⁶⁸ are observed. Meanwhile, the positive or negative bands in the hydroxyl region (bands at 3740 and 3680 cm^{-1}) originated from the changes in the coordination number of iron sites during NH_3 -SCR reaction. Compared with the spectra obtained in NO - O_2 , NH_3 - O_2 and NH_3 - NO , NH and nitroxyl HNO species are observed as new species in NH_3 -SCR and they should be related to the high activity of Fe-beta. According to the spectroscopy results in Fig. 12, we simply assume that the adsorbed NH and nitroxyl HNO species are produced from the interaction between ammonia and nitrite species ($\text{NH}_3 + *NO_2 \rightarrow *HNO + *NH$); however, the detailed reaction chemistry could not be disclosed at this time.

The *in situ* DRIFT spectra of NH_3 -SCR over Fe-beta at different reaction temperatures are shown in Fig. 13. At a low reaction temperature of 473 K, N_xO_y species (nitro compounds

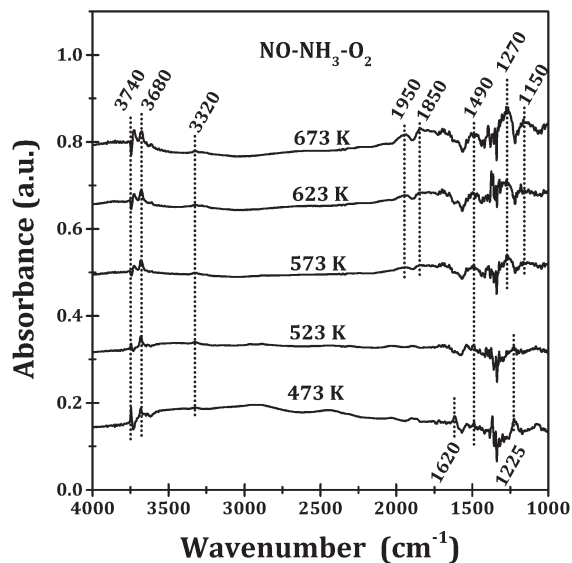


Fig. 13 *In situ* DRIFT spectra of NH_3 -SCR over Fe-beta at different reaction temperatures. Reaction conditions: $\text{NO} = 1000$ ppm; $\text{NH}_3 = 1000$ ppm; $\text{O}_2 = 10\%$; ~ 25 mg catalyst; total flow rate of 25 mL min^{-1} ; GHSV = $\sim 60\,000$ per h.

at 1620 cm^{-1} ; nitroxyl HNO species at 1490 cm^{-1} ; nitrite species at 1225 cm^{-1}) and adsorbed NH species (weak IR band at 3320 cm^{-1}) are identified as dominating surface species formed. The NH_3 -SCR reaction rate at this temperature is very low (Fig. 10), indicating that the reaction between these adsorbed species is difficult. With increasing reaction temperatures, the types of adsorbed N_xO_y species changes and their intensities increase distinctly. The much higher NH_3 -SCR reaction rates (Fig. 9) suggest the easier reaction between these species. Meanwhile, adsorbed mono-nitrosyls (IR bands at 1850 cm^{-1}) could be observed at 573–673 K. The appearance of unoxidized mono-nitrosyls on the active iron sites hints to the fact that the oxidation of NO is a key step in NH_3 -SCR catalyzed by Fe-beta.

Integrating the *in situ* DRIFT spectra and the activity data, some key points regarding the NH_3 -SCR over Al-free Fe-beta could be drawn. Firstly, the NH_3 -SCR reaction occurs solely on the iron sites in Fe-beta, *i.e.* the isolated iron sites stabilized by the zeolite framework. Even though the role of framework aluminium species and associated Brønsted acid sites in NH_3 -SCR could not be totally excluded in Fe-zeolite catalysts, our experimental results indicate that NH_3 -SCR reaction can proceed, with high reaction rates, in the absence of framework aluminium species and associated Brønsted acid sites. Secondly, the reactants NO, NH_3 and O_2 interact with iron sites and accordingly change their coordination numbers, as reflected by the formation and consumption of hydroxyls bounded to the iron sites. These observations agree well with previous reports where the Fe^{3+} - Fe^{2+} redox cycle has been proposed.^{19,72} Finally, adsorbed NH , N_xO_y and HNO species are dominating reactive species formed on Fe-beta during NH_3 -SCR, and N_2 and H_2O could be produced from the reaction between them. During the process, the oxidation of NO to surface N_xO_y species is a key step in the whole reaction.

4. Conclusion

An Al-free Fe-beta zeolite has been successfully prepared *via* a two-step post-synthesis metallation strategy, consisting of creating vacant T sites by dealumination of commercial H-beta and subsequent dry impregnation of the resulting Si-beta with organometallic ferrocene. Characterization results from TEM, H_2 -TPR and UV-vis spectroscopy reveal that iron species are incorporated into the framework of zeolite and most of the iron species exist as isolated ferric ions in Fe-beta. No Brønsted acid sites are present in Fe-beta due to the complete removal of the framework aluminium species, and strong Lewis acids are created through the incorporation of iron species into the BEA framework, as verified by analysis results from NH_3 -TPD and FTIR spectroscopy of pyridine adsorption.

The as-prepared Fe-beta exhibits good catalytic activity, comparable with reference Fe-H-beta prepared *via* solid-state ion exchange, in NH_3 -SCR reaction. Typically, a nitrogen oxide conversion of $>85\%$ can be achieved at 623–723 K under our reaction conditions, *i.e.* GHSV = 60 000 per h, $\text{NO} = 1000$ ppm, $\text{NH}_3 = 1000$ ppm, $\text{O}_2 = 10\%$, $\text{SO}_2 = 50$ ppm, $\text{H}_2\text{O} = 10\%$, He balance. The distinct advantage of Fe-beta over other Fe-zeolites reported for NH_3 -SCR is its durability; a nitrogen oxide conversion of $>90\%$ can be maintained for over 400 h at 673 K. The remarkable durability of Fe-beta can be explained from the absence of framework aluminium species and the stabilization of active iron species by the zeolite framework, as verified by TEM and UV-vis analysis.

The as-prepared Fe-beta with well-defined iron sites and without Brønsted acid sites is an ideal model catalyst for the NH_3 -SCR mechanism study. *In situ* DRIFT spectroscopy results reveal that adsorbed NH , N_xO_y and HNO species are dominating reactive species formed on Fe-beta during NH_3 -SCR, where N_2 and H_2O are produced from the reaction between them. The oxidation of NO is established as a key step in NH_3 -SCR catalyzed by Fe-beta.

Acknowledgements

This work is financially supported by the National Natural Science Foundation of China (21373119 and 21421001), the Municipal Natural Science Foundation of Tianjin (13RCGFGX01124, 14JCQNJC05700 and 13JCQNJC05900), and the Ministry of Education of China (IRT13022).

Notes and references

- X. B. Feng and W. K. Hall, *J. Catal.*, 1997, **166**, 368–376.
- F. Heinrich, C. Schmidt, E. Löffler, M. Menzel and W. Grünert, *J. Catal.*, 2002, **212**, 157–172.
- R. Brosius, P. Bazin, F. Thibault-Starzyk and J. A. Martens, *J. Catal.*, 2005, **234**, 191–198.
- M. Schwidder, M. S. Kumar, K. Klementiev, M. M. Pohl, A. Brückner and W. Grünert, *J. Catal.*, 2005, **231**, 314–330.
- M. S. Kumar, M. Schwidder, W. Grünert, U. Bentrup and A. Brückner, *J. Catal.*, 2006, **239**, 173–186.

- 6 R. Q. Long and R. T. Yang, *J. Am. Chem. Soc.*, 1999, **121**, 5595–5596.
- 7 A. Z. Ma and W. Grünert, *Chem. Commun.*, 1999, 71–72.
- 8 R. Q. Long and R. T. Yang, *J. Catal.*, 2002, **207**, 224–231.
- 9 G. Qi and R. T. Yang, *Appl. Catal., B*, 2005, **60**, 13–22.
- 10 G. Delahay, D. Valade, A. Guzmán-Vargas and B. Coq, *Appl. Catal., B*, 2005, **55**, 149–155.
- 11 A. Grossale, I. Nova and E. Tronconi, *Catal. Today*, 2008, **136**, 18–27.
- 12 M. Iwasaki, K. Yamazaki, K. Banno and H. Shinjoh, *J. Catal.*, 2008, **260**, 205–216.
- 13 M. Høj, M. J. Beier, J. Grunwaldt and S. Dahl, *Appl. Catal., B*, 2009, **93**, 166–176.
- 14 S. Brandenberger, O. Kröcher, A. Wokaun, A. Tissler and R. Althoff, *J. Catal.*, 2009, **268**, 297–306.
- 15 S. Brandenberger, O. Kröcher, M. Casapu, A. Tissler and R. Althoff, *Appl. Catal., B*, 2011, **101**, 649–659.
- 16 S. Brandenberger, O. Kröcher, A. Tissler and R. Althoff, *Appl. Catal., B*, 2010, **95**, 348–357.
- 17 M. Iwasaki, K. Yamazaki and H. Shinjoh, *Appl. Catal., B*, 2011, **102**, 302–309.
- 18 P. Sazama, B. Wichterlová, E. Tábor, P. Štátný, N. K. Sathu, Z. Sobalík, J. Dědeček, Š. Sklenák, P. Klein and A. Vondrová, *J. Catal.*, 2014, **312**, 123–138.
- 19 A. Boubnov, H. W. P. Carvalho, D. E. Doronkin, T. Günter, E. Gall, A. J. Atkins, C. R. Jacob and J.-D. Grunwaldt, *J. Am. Chem. Soc.*, 2014, **136**, 13006–13015.
- 20 M. Devadas, O. Kröcher, M. Elsener, A. Wokaun, N. Söger, M. Pfeifer, Y. Demel and L. Mussmann, *Appl. Catal., B*, 2006, **67**, 187–196.
- 21 A. Grossale, I. Nova, E. Tronconi, D. Chatterjee and M. Weibel, *J. Catal.*, 2008, **256**, 312–322.
- 22 M. Schwidder, S. Heikensa, A. De Toni, S. Geisler, M. Berndt, A. Brückner and W. Grünert, *J. Catal.*, 2008, **259**, 96–103.
- 23 M. Iwasaki and H. Shinjoh, *Appl. Catal., A*, 2010, **390**, 71–77.
- 24 M. Colombo, I. Nova, E. Tronconi, V. Schmeißer, B. Bandler-Konrad and L. Zimmermann, *Appl. Catal., B*, 2012, **111–112**, 106–118.
- 25 X. Shi, F. Liu, L. Xie, W. Shan and H. He, *Environ. Sci. Technol.*, 2013, **47**, 3293–3298.
- 26 G. Delahay, M. Mauvezin, B. Coq and S. Kieger, *J. Catal.*, 2001, **202**, 156–162.
- 27 J. Pérez-Ramírez, F. Kapteijn and A. Brückner, *J. Catal.*, 2003, **218**, 234–238.
- 28 M. Yoshida, T. Nobukawa, S. Ito, K. Tomishige and K. Kunimori, *J. Catal.*, 2004, **223**, 454–464.
- 29 T. Nobukawa, M. Yoshida, K. Okumura, K. Tomishige and K. Kunimori, *J. Catal.*, 2005, **229**, 374–388.
- 30 K. Sun, H. Xia, E. Hensen, R. van Santen and C. Li, *J. Catal.*, 2006, **238**, 186–195.
- 31 D. Kaucký, Z. Sobalík, M. Schwarze, A. Vondrová and B. Wichterlová, *J. Catal.*, 2006, **238**, 293–300.
- 32 J. Kyu Lee, Y. J. Kim, H.-J. Lee, S. H. Kim, S. J. Cho, I.-S. Nam and S. B. Hong, *J. Catal.*, 2011, **284**, 23–33.
- 33 X. Zhang, Q. Shen, C. He, C. Ma, J. Cheng, L. Li and Z. Hao, *ACS Catal.*, 2012, **4**, 512–520.
- 34 L. V. Pirutko, V. S. Chernyavsky, A. K. Uriarte and G. I. Panov, *Appl. Catal., A*, 2002, **227**, 143–157.
- 35 E. J. M. Hensen, Q. Zhu and R. A. van Santen, *J. Catal.*, 2003, **220**, 260–264.
- 36 I. Yuranov, D. A. Bulushev, A. Renken and L. Kiwi-Minsker, *J. Catal.*, 2004, **227**, 138–147.
- 37 E. J. M. Hensen, Q. Zhu, R. A. J. Janssen, P. C. M. M. Magusin, P. J. Kooyman and R. A. van Santen, *J. Catal.*, 2005, **233**, 123–135.
- 38 J. Pérez-Ramírez and A. Gallardo-Llamas, *J. Catal.*, 2004, **223**, 382–388.
- 39 O. Sánchez-Galofré, Y. Segura and J. Pérez-Ramírez, *J. Catal.*, 2007, **249**, 123–133.
- 40 W. Wei, J. A. Moulijn and G. Mul, *J. Catal.*, 2009, **262**, 1–8.
- 41 G. Wu, F. Hei, N. Guan and L. Li, *Catal. Sci. Technol.*, 2013, **3**, 1333–1342.
- 42 J. H. Yun and R. F. Lobo, *J. Catal.*, 2014, **312**, 263–270.
- 43 I. Nova and E. Tronconi, *Urea-SCR Technology for deNOx After Treatment of Diesel Exhausts*, Springer, New York, 2004.
- 44 K. Krishna and M. Makkee, *Catal. Today*, 2006, **114**, 23–30.
- 45 T. J. Toops, K. Nguyen, A. L. Foster, B. G. Bunting, N. A. Ottinger, J. A. Pihl, E. W. Hagaman and J. Jiao, *Catal. Today*, 2010, **151**, 257–265.
- 46 S. Dzwigaja and M. Che, *Catal. Today*, 2001, **169**, 232–241.
- 47 S. Dzwigaj, J. Janas, J. Gurgul, R. P. Socha, T. Shishido and M. Che, *Appl. Catal., B*, 2009, **85**, 131–138.
- 48 B. Tang, W. Dai, G. Wu, N. Guan, L. Li and M. Hunger, *ACS Catal.*, 2014, **4**, 2801–2810.
- 49 B. Tang, W. Dai, X. Sun, G. Wu, N. Guan, M. Hunger and L. Li, *Green Chem.*, 2015, **17**, 1744–1755.
- 50 C. A. Emeis, *J. Catal.*, 1993, **141**, 347–354.
- 51 K. Nakamoto, *Infrared and Raman Spectra of Inorganic Coordination Compounds*, Wiley, New York, 1997.
- 52 R. Buzzoni, S. Bordiga, G. Ricchiardi, C. Lamberti, A. Zecchina and G. Bellussi, *Langmuir*, 1996, **12**, 930–940.
- 53 R. S. Assary, L. A. Curtiss and J. A. Dumesic, *ACS Catal.*, 2013, **3**, 2694–2704.
- 54 W. Dai, C. Wang, B. Tang, G. Wu, N. Guan, Z. Xie, M. Hunger and L. Li, *ACS Catal.*, 2016, **6**, 2955–2964.
- 55 G. D. Pirngruber, P. K. Roy and R. Prins, *Phys. Chem. Chem. Phys.*, 2006, **8**, 3939–3950.
- 56 M. S. Kumar, M. Schwidder, W. Grünert and A. Brückner, *J. Catal.*, 2004, **227**, 384–397.
- 57 G. Berlier, C. Lamberti, M. Rivallan and G. Mul, *Phys. Chem. Chem. Phys.*, 2010, **12**, 358–364.
- 58 G. Mul, J. Pérez-Ramírez, F. Kapteijn and J. A. Moulijn, *Catal. Lett.*, 2002, **80**, 129–138.
- 59 R. W. Joyner and M. Stockenhuber, *J. Phys. Chem. B*, 1999, **103**, 5963–5976.
- 60 A. H. Øygardena and J. Pérez-Ramírez, *Appl. Catal., B*, 2006, **65**, 163–167.
- 61 S. Dzwigaj, J. Janas, W. Rojek, L. Stievano, F. E. Wagner, F. Averseng and M. Che, *Appl. Catal., B*, 2009, **86**, 45–52.
- 62 H. Liu, J. Wang, T. Yu, S. Fan and M. Shen, *Catal. Sci. Technol.*, 2014, **4**, 1350–1356.
- 63 J. Kim, A. Jentys, S. M. Maier and J. A. Lercher, *J. Phys. Chem. C*, 2013, **117**, 986–993.

- 64 S. M. Maier, A. Jentys, M. Janousch, J. A. van Bokhoven and J. A. Lercher, *J. Phys. Chem. C*, 2012, **116**, 5846–5856.
- 65 S. A. Skarlis, D. Berthout, A. Nicolle, C. Dujardin and P. Granger, *J. Phys. Chem. C*, 2013, **117**, 7154–7169.
- 66 Y. He, M. E. Ford, M. Zhu, Q. Liu, Z. Wu and I. E. Wachs, *Appl. Catal., B*, 2016, **188**, 123–133.
- 67 N. Macleod and R. M. Lambert, *Chem. Commun.*, 2003, 1300–1301.
- 68 K. Hadjiivanov, *Catal. Rev.: Sci. Eng.*, 2000, **42**, 71–144.
- 69 E. Hecceg, K. Mudiyansele and M. Trenary, *J. Phys. Chem. B*, 2005, **109**, 2828–2835.
- 70 G. Ramis, L. Yi, G. Busca, M. Turco, E. Kotur and R. Willey, *J. Catal.*, 1995, **157**, 523–535.
- 71 M. P. Ruggeri, T. Selleri, M. Colombo, I. Nova and E. Tronconi, *J. Catal.*, 2014, **311**, 266–270.
- 72 S. M. Maier, A. Jentys, E. Metwalli, P. Müllerbuschbaum and J. A. Lercher, *J. Phys. Chem. Lett.*, 2011, **2**, 950–955.